Kovove Mater. 48 2010 327–336
DOI: 10.4149/km_2010_5_327

Numerical simulation of induction heating of a rod semiproduct for the process of rotary spin extrusion

M. Behúlová[1]*, B. Mašek[2,3], L. W. Meyer[3]

[1] *Slovak University of Technology in Bratislava, Faculty of Materials Science and Technology in Trnava, Paulínska 16, 917 24 Trnava, Slovak Republic*
[2] *University of West Bohemia in Pilsen, Faculty of Mechanical Engineering, FORTECH, Univerzitní 8, 306 14 Pilsen, Czech Republic*
[3] *TU Chemnitz, Fakultät für Maschinenbau, LWM, Erfenschlager Str. 73, D-09107 Chemnitz, Deutschland*

Received 16 August 2006, received in revised form 2 March 2009, accepted 30 June 2010

Abstract

Technology of rotary spin extrusion is intended for the manufacturing of semiproducts of hollow shafts for motor vehicles. It belongs to the advanced forming processes using which semiproducts with outstanding material properties can be produced applying a unique incremental deformation technique at controlled temperatures.

In order to ensure a high efficiency of the process and to improve the conditions for plastic material flow, a system of induction heating and water spray cooling is expected to be integrated to the process chain. According to the virtual design for arrangement of heating and cooling components, the simulation model for numerical analysis of electro-magnetic and temperature fields in a rod semiproduct from the 20MoCrS4 steel was developed. Based on numerical experiments and analysis of temperature fields in heated rod semiproduct, the parameters of induction heating and consecutive surface cooling were defined.

K e y w o r d s: rotary spin extrusion, induction heating, numerical simulation, electro-magnetic fields, temperature fields

1. Introduction

Recently, a large series of new forming technologies allowing extending the range of formed products have emerged. These usually concern not only an effective achievement of required dimensions but also utilizing the possibility to improve material properties at the same time. With a complex interconnection of optimal parameters of construction, technology and material, products or semiproducts with generally better utility properties can be manufactured.

The technology of rotary spin extrusion [1–5] is a good example. This technology allows nearly wasteless production of hollow components from massive semiproducts applying incremental forming. With the use of controlled temperature fields during the forming process and semiproduct cooling, it is possible to obtain not only effective, construction-optimised shapes but also suitable structures distinguished by very good dynamical properties that are unreachable through conventional procedures.

2. Problem description

Technology of rotary spin extrusion developed at the Chemnitz University of Technology is dedicated to manufacturing of hollow shafts for vehicle gear boxes [1–6]. This technology takes advantage of a very efficient incremental forming process. Applying unique incremental-deformation method with roll-off tools enables production of hollow and internally profiled parts directly from cylindrical rod semiproducts with minimal material losses, which are usually connected with conventional machining such as drilling or turning.

The principle of the rotary spin extrusion is based on the deformation effect of three rollers located on

*Corresponding author: tel.: +421 33 5511601; fax: +421 33 5511758; e-mail address: maria.behulova@stuba.sk

Table 1. Chemical composition of the 20MoCrS4 steel (wt.%)

C	Mn	Cr	Mo	Ni	Si	P	S	Al	V	Cu	W	Co	Nb
0.22	0.87	0.73	0.40	0.11	0.24	0.02	0.03	0.03	0.01	0.13	0.02	0.02	0.01

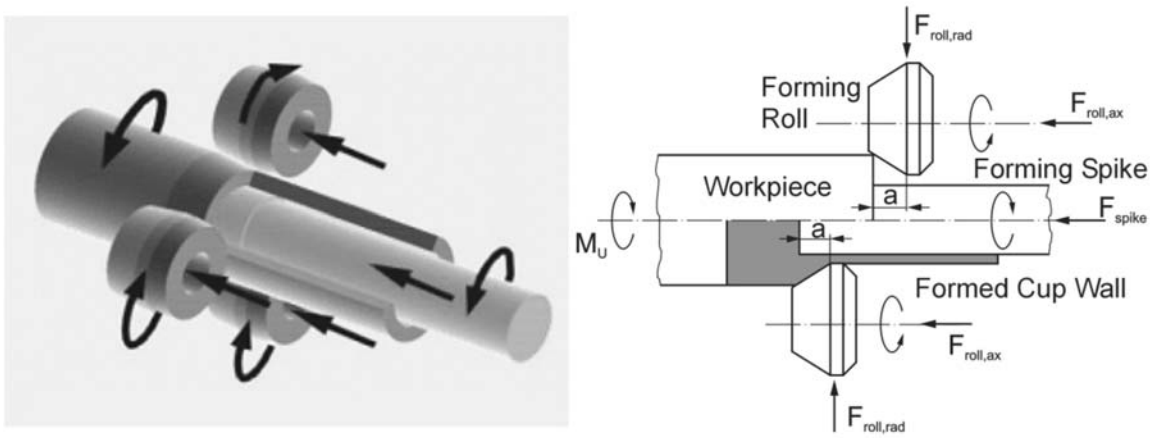

Fig. 1. The principle of the process of rotary spin extrusion [1, 3].

Fig. 2. Variable internal profiles of hollow shafts from different materials produced by rotary spin extrusion [2].

the diameter of the forming zone that form the outer shaft contour (Fig. 1). At the same time, the spike is pressed in the axial direction into the rod to form the inner shaft contour. Thus, the material displaced by the rollers and the forming spike runs off axially forming a cup wall. The rotational movements of the spike and rollers are not generated by separate driving mechanisms but they result from the friction. Because the spike is rotating with the same angular velocity as the formed rod semiproduct, it is possible to produce even incircular or profiled inner shapes such as polygons, internal toothing, multiple-spline profiles using accordingly designed forming spikes (Fig. 2). In only one forming step, the semi-finished hollow shafts with a length-diameter ratio up to 20 can be produced [6].

Depending on the material of the formed semiproduct and required accuracy of internal and external shapes, the rotary spin extrusion can be used as a cold-, warm- or hot-forming technique. The high-strength steels are supposed to be treated by increased temperatures in order to improve conditions for plastic material flow what results in considerable reduction of the punch power [2, 5]. Moreover, the exploitation of incremental deformations at higher temperatures exhibits positive consequences on the microstructure and the material properties, particularly on the ductility, ultimate and impact strength. In this reason, wide range of strategies of thermo-mechanical treatment of steels has been examined and verified experimentally for the technology of spin extrusion [8–13].

In this work, the processes of induction heating and cooling of a rod semiproduct from the 20MoCrS4 steel for the rotary spin extrusion are investigated using numerical simulation of electro-magnetic and temperature fields by the program code ANSYS 10.0. The main aim of the FEM simulation is to design the necessary inductor power and parameters of water jet and air cooling for the required temperature distribution in a rod semiproduct at the end of the initial stage of spin extrusion process before the billet starts to be in the contact with rollers and spike (Fig. 3). For the considered 20MoCrS4 steel (Table 1), the desired axial temperature in front of the spike at this time is from 700 ℃ to 750 ℃ while the surface temperatures under rollers shall be not higher than 600 ℃ and the maximum billet temperatures under the inductor should not exceed 1200 ℃.

3. Mathematical model

In induction heating processes, an alternating cur-

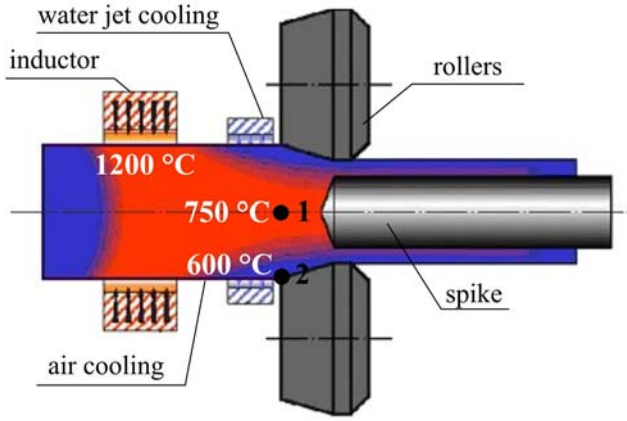

Fig. 3. Virtual model of induction heating and cooling in the process of rotary spin extrusion with required temperature distribution.

rent is passed through the inductor coil, creating an alternating magnetic field. A billet placed into this magnetic field becomes a part of the electro-magnetic circuit. In the billet, eddy currents are induced and the material is heated up due to resistive and hysteresis losses. The induced current and consequently the generated heat are not uniformly distributed throughout the billet. Around 63 % of induced current and 87 % of generated heat are concentrated in the outer region called penetration or skin depth [14–16]. The penetration depth is defined as the distance from the billet surface at which the current density decreases exponentially to the 1/e of its value at the surface. At the distance of one skin depth, the current is equal to about 37 % and the power density reaches approximately to 13 % of their values at the surface.

The skin depth δ depends on electric and magnetic properties of material and mainly on the frequency of current in the inductor coil. It can be calculated from the relationship [15]

$$\delta = \sqrt{\frac{\rho_{\mathrm{el}}}{\pi \mu_0 \mu_{\mathrm{r}} f}}, \tag{1}$$

where ρ_{el} is the resistivity of a billet material, μ_0 is the permeability of vacuum ($\mu_0 = 4\pi{\cdot}10^{-7}\,\mathrm{H\,m^{-1}}$), μ_{r} is the relative permeability and f is the frequency of the source current.

Numerical simulation of induction heating processes requires solving coupled electro-magnetic and transient thermal problem because of temperature dependent electric and magnetic material properties, time, frequency and material dependent loading. The material properties in both electro-magnetic and thermal analyses vary very strongly with temperature, position of inductor and cooling zones are functions of time. In addition, the boundary conditions are temperature dependent as well.

3.1. Governing equations for the electro-magnetic field

The governing equations for the electro-magnetic analysis can be derived from the classical four Maxwell's equations [15–16]:

$$\mathrm{rot}\,\boldsymbol{H} = \boldsymbol{j} + \frac{\partial \boldsymbol{D}}{\partial t}, \tag{2}$$

$$\mathrm{rot}\,\boldsymbol{E} = -\frac{\partial \boldsymbol{B}}{\partial t}, \tag{3}$$

$$\mathrm{div}\,\boldsymbol{D} = \rho_{\mathrm{e}}, \tag{4}$$

$$\mathrm{div}\,\boldsymbol{B} = 0, \tag{5}$$

where $\boldsymbol{D}$ is the vector of electric flux density, $\boldsymbol{E}$ is the electric field intensity, $\boldsymbol{B}$ is the magnetic flux density, $\boldsymbol{H}$ is the magnetic field intensity, ρ_{e} is the free charge density, $\boldsymbol{j}$ the current density and t is the time.

The field vectors $\boldsymbol{D}$ and $\boldsymbol{E}$ and also $\boldsymbol{B}$ and $\boldsymbol{H}$ are related by material properties through the functions referred as the constitutive equations

$$\boldsymbol{D} = \varepsilon\,\boldsymbol{E}, \tag{6}$$

$$\boldsymbol{B} = \mu\,\boldsymbol{H}, \tag{7}$$

$$\boldsymbol{j} = \sigma\,\boldsymbol{E}, \tag{8}$$

in which σ is the electrical conductivity, ε is the permitivity given by the product of the vacuum permitivity ε_0 and the relative permitivity ε_{r} ($\varepsilon = \varepsilon_0\varepsilon_{\mathrm{r}}$) and μ is the magnetic permeability ($\mu = \mu_0\mu_{\mathrm{r}}$).

Since $\boldsymbol{B}$ satisfies a zero divergence condition, $\mathrm{div}\,\boldsymbol{B} = 0$, the magnetic vector potential $\boldsymbol{A}$ can be defined by the relationship

$$\boldsymbol{B} = \mathrm{rot}\,\boldsymbol{A}. \tag{9}$$

Then the Maxwell's equations (2)–(5) lead to following expressions of the diffusion equation for electrically conductive (10) and non-conductive materials (11), respectively:

$$\Delta\boldsymbol{A} - \varepsilon\frac{\partial^2 \boldsymbol{A}}{\partial t^2} - \mu\sigma\frac{\partial \boldsymbol{A}}{\partial t} = 0, \tag{10}$$

$$\Delta\boldsymbol{A} - \mu\varepsilon\frac{\partial^2 \boldsymbol{A}}{\partial t^2} = 0. \tag{11}$$

For time harmonic electro-magnetic fields, the current density and magnetic vector potential vary with time according to the relationships

$$\boldsymbol{j} = \boldsymbol{j}_0\,\mathrm{e}^{\mathrm{i}\omega t}, \tag{12}$$

$$\boldsymbol{A} = \boldsymbol{A}_0\,\mathrm{e}^{\mathrm{i}\omega t}, \tag{13}$$

where ω is the angular frequency.

For axisymmetric condition, the magnetic field intensity $\boldsymbol{H}$ acts in the axial direction, the magnetic vector potential $\boldsymbol{A}$ and eddy current have only one component in peripheral direction.

Using Eqs. (12) and (13) and axisymmetric conditions, the Eqs. (10) and (11) can be rewritten in the cylindrical coordinates (r, φ, z) to the form

$$\frac{\partial^2 A}{\partial r^2} + \frac{1}{r}\frac{\partial A}{\partial r} - \omega\sigma\mu A = 0, \tag{14}$$

$$\frac{\partial^2 A}{\partial r^2} + \frac{1}{r}\frac{\partial A}{\partial r} + \omega^2\varepsilon\mu A = 0. \tag{15}$$

3.2. Governing equations for the temperature field

The temperature fields are governed by the Fourier-Kirchhoff's heat diffusion equation [17, 18], which expresses the energy conservation law for heat conduction

$$c\rho\frac{\partial T}{\partial t} = \operatorname{div}\left(\boldsymbol{\lambda}\operatorname{grad} T\right) + q_{\mathrm{v}}, \tag{16}$$

or for the heat conduction in an isotropic material at axisymmetric conditions considering the heat source movement in z-direction:

$$c\rho\frac{\partial T}{\partial t} = \lambda\left(\frac{\partial^2 T}{\partial r^2} + \frac{1}{r}\frac{\partial T}{\partial r} + \frac{\partial^2 T}{\partial z^2}\right) + q_{\mathrm{v}}, \tag{17}$$

where ρ is the density, c is the specific heat, $\boldsymbol{\lambda}$ is the thermal conductivity tensor, $\lambda = \lambda_x = \lambda_y = \lambda_z$ is the thermal conductivity of an isotropic material and q_{v} is the volume heat source density, i. e. the heat generated per unit time in a unit volume. In induction heating this term depends on the Joule heat generation in the heated material due to the eddy currents.

Usually, three kinds of boundary conditions for heat diffusion equation (16) are used. The boundary condition of the first kind is determined by the given surface temperature as a function of position, $\boldsymbol{r}$, and time, t:

$$T = f_1(\boldsymbol{r}, t) \quad \text{at the surface } \mathrm{S}_1. \tag{18}$$

The boundary condition of the second kind expresses the surface conductive heat flux as a function of position and time:

$$\boldsymbol{q} = -\lambda\frac{\partial T}{\partial \boldsymbol{n}} = f_2(\boldsymbol{r}, t) \quad \text{at the surface } \mathrm{S}_2, \tag{19}$$

where $\partial T/\partial \boldsymbol{n}$ denotes differentiation along the outward-drawn normal $\boldsymbol{n}$ at the boundary surface S_2. This condition is applied as well as at the adiabatic (insulated) surfaces or as a symmetry condition when the surface heat flux is zero.

Most frequently, a boundary condition of the third kind is used. According to this condition, the surface conduction heat flux is equal to the convection heat flux

$$-\lambda\frac{\partial T}{\partial \boldsymbol{n}} = h\left(T_{\mathrm{w}} - T_{\mathrm{f}}\right) \quad \text{at the surface } \mathrm{S}_3, \tag{20}$$

where h is the heat transfer coefficient, T_{w} is the surface temperature and T_{f} is the fluid temperature.

To apply this condition, it is necessary to define the surrounding temperature and the heat transfer coefficient, which can be time and/or temperature dependent. Usually, the combined heat transfer coefficient includes the influence of convection and radiation, so it is given by the sum of convection heat transfer coefficient h_{C} and radiation heat transfer coefficient h_{R}:

$$h = h_{\mathrm{C}} + h_{\mathrm{R}} = h_{\mathrm{C}} + \frac{\varepsilon_{\mathrm{e}}\sigma_0\left(T_{\mathrm{w}}^4 - T_{\mathrm{f}}^4\right)}{T_{\mathrm{w}} - T_{\mathrm{f}}}, \tag{21}$$

where ε_{e} is the emissivity and σ_0 is the Stefan-Boltzmann's constant.

4. Solution procedure

To solve the problem of induction heating for the process of rotary spin extrusion, the sequential field-coupling method [19] provided by the program code ANSYS 10.0 was applied. A special user subroutine was developed to control the field coupling.

According to Fig. 4, the Joule heat generation data computed by the harmonic electro-magnetic analysis are applied as a loading for the transient thermal analysis in order to predict the time-dependent temperature distribution. As the temperature field influences the electro-magnetic field through the temperature dependent electro-magnetic properties, the computed temperatures enter as a load for the electromagnetic analysis. Moreover, inductor position has to be up-dated by dynamic induction heating.

The methodology for the analysis of temperature fields by induction heating was verified using the temperature measurement by static and dynamic induction heating of a rod semiproduct [20].

5. Simulation model

5.1. Geometrical model and FEM mesh

Based on the virtual model of heating and cooling zones locations [21], the geometrical model illustrated

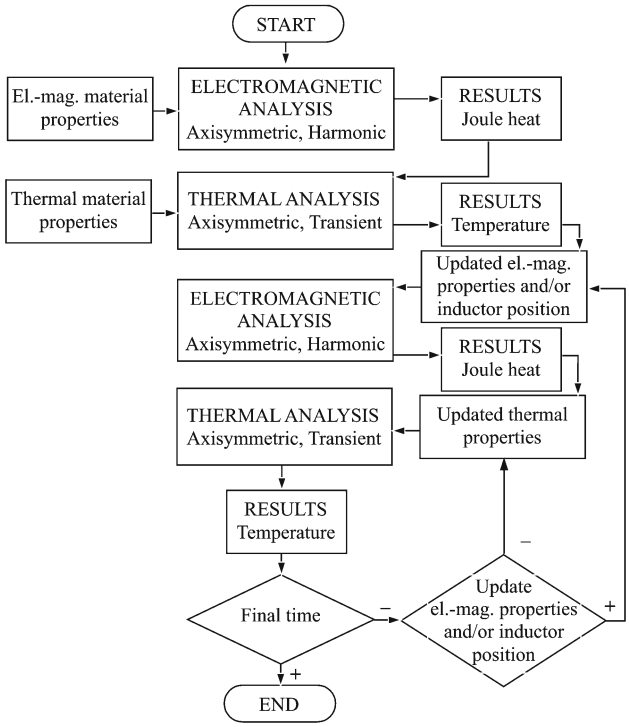

Fig. 4. Scheme of solution procedure using the sequential field coupling in ANSYS.

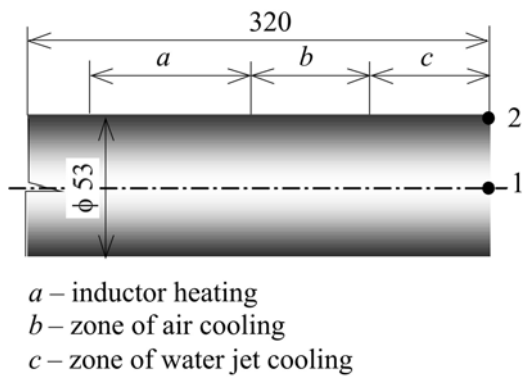

Fig. 5. Geometrical model with the lengths of heating and cooling zones.

in Fig. 5 was prepared. Induction heating is supposed in the zone with the length of $a = 38$ mm by a three--turn water cooled induction coil (Fig. 6). The zone of air cooling (b) located directly behind the inductor serves for the heat flow to reach the central parts of a heated billet before intensive water jet cooling of the billet surface in order to achieve required surface temperatures under rollers. The prescribed total length of cooling zones ($b + c$) is 60 mm. In the starting position, the billet head is inserted into a half of inductor coil (19 mm), so its distance from the spike is 79 mm. Assuming the feed rate of 3 mm s^{-1}, the billet will

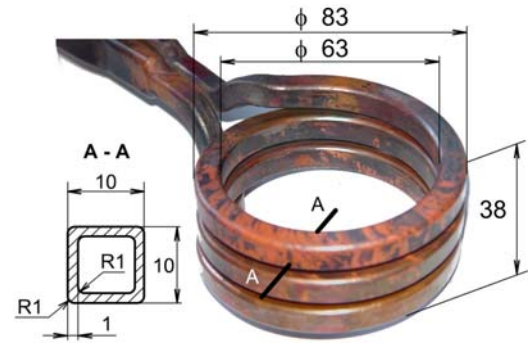

Fig. 6. Geometrical characteristics of induction coil.

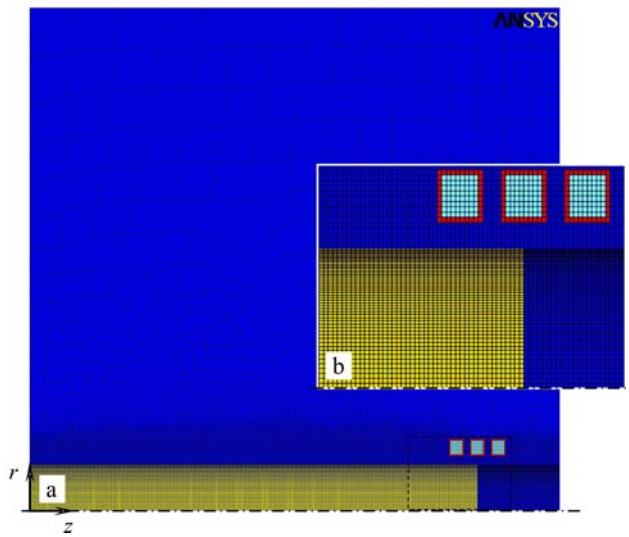

Fig. 7. Axisymmetric FE model for electro-magnetic and thermal analysis (a) with a detail of generated mesh and initial position of inductor coil (b).

come into the contact with the spike in the time of 26.33 seconds after the induction heating start up.

Finite element meshes for electro-magnetic analysis and thermal analyses (Fig. 7a) were generated using linear axisymmetric elements. To take into account the skin depth, the progressive mesh in the cylindrical billet was created. The mesh density near the surface is significantly higher than in the middle parts (Fig. 7b) what corresponds to the exponential decay in induced eddy currents and consequently in the decrease of Joule heat generation towards the billet axis. The detail in Fig. 7b shows also the initial position of the inductor coil.

5.2. Material properties

Material properties of 20MoCrS4 steel (Table 2) were considered to be temperature dependent. Electrical properties including the temperature dependent

Table 2. Material properties of 20MoCrS4 steel

Material property	Temperature (°C)								
	0	100	200	400	600	800	900	1000	1200
$\rho_{el} \times 10^8$ (Ω m)	61.8	69.4	77.0	80.0	95.1	124.5	140.0	152.0	168.0
λ (W m^{-1} K^{-1})	44.8	43.6	41.9	36.8	32.9	29.6	28.5	28.7	29.2
c (J kg^{-1} K^{-1})	475	489	495	518	580	585	600	620	650
ρ (kg m^{-3})	7850	7822	7793	7729	7656	7616	7560	7560	7560
ε_e (–)					0.56				

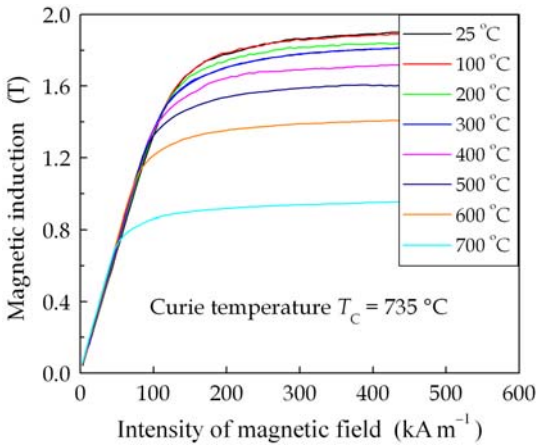

Fig. 8. Temperature dependent *B-H* curves of 20MoCrS4 steel.

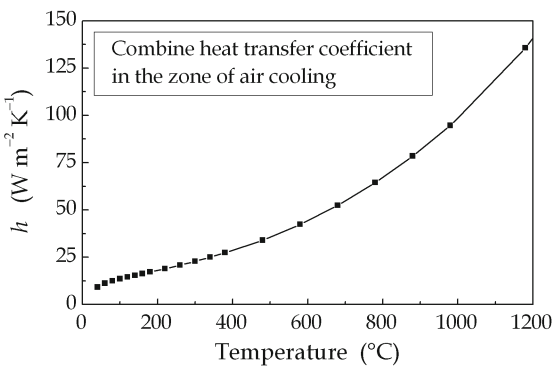

Fig. 9. Combined heat transfer coefficient in the zone of air cooling in the dependence on billet surface temperature.

electrical resistivity (Table 2) and *B-H* curves (Fig. 8) were measured at the Institute of Experimental Physics of the Slovak Academy of Sciences in Košice. User subroutine was developed to involve the *B-H* curves for different temperatures into the ANSYS computation model. The method of modified specific heat capacity [19, 22] was adopted to take into account the latent heat of austenitic transformation.

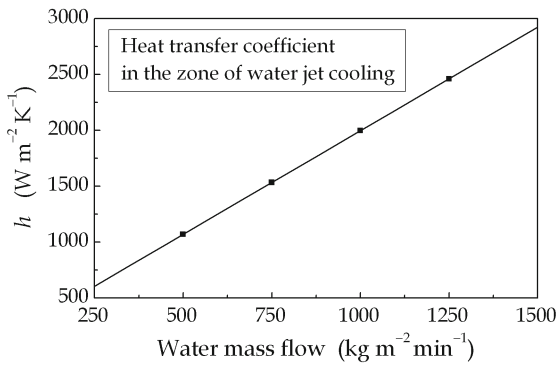

Fig. 10. Dependence of heat transfer coefficient in the zone of water spray cooling on water mass flow [20].

5.3. Loads, initial and boundary conditions

The initial temperature of the billet was supposed to be 20 °C. In the billet axis, the symmetry boundary conditions were applied, i. e. the magnetic vector potential and the heat flux were set to zero. Induction heating with the current density from 1.3×10^8 A m^{-2} to 1.4×10^8 A m^{-2} and the relatively low frequency of 2 kHz was proposed [21] according to the requirement to heat particularly the central parts of a billet. With the frequency decrease, the skin depth increases what contributes to the faster heating of the rod central parts but efficiency of induction heating can fall down [23]. In this case of induction heating of the billet with 53 mm in diameter, the efficiency of heating is sufficiently high [21].

In the zone of air cooling, the heat extraction from the billet by mechanisms of free convection and radiation were supposed and modelled applying the time and temperature dependent boundary condition of the third kind. The combined heat transfer coefficient (Fig. 9) was calculated from the Eq. (21) as a function of the billet surface temperature using classical criterial equations [17, 24] and surrounding temperature of 25 °C.

The exact theoretical determination of the heat transfer coefficient in the process of water jet cooling is very complicated. Therefore, the experimental results

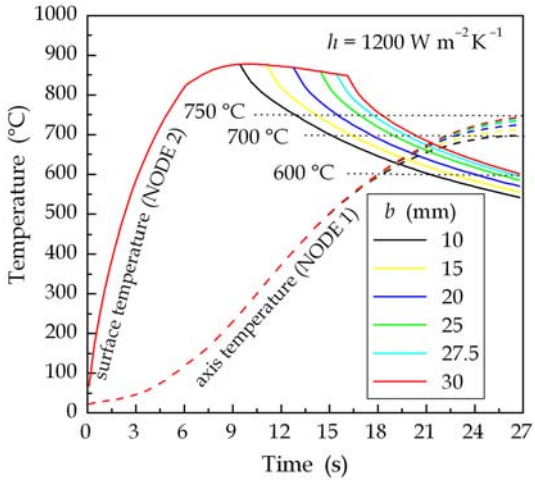

Fig. 11. Temperature histories in the node 1 (dashed lines) and in the node 2 (solid lines) for different lengths of air cooling zones b and water mass flow of 570 kg m^{-2} min^{-1}.

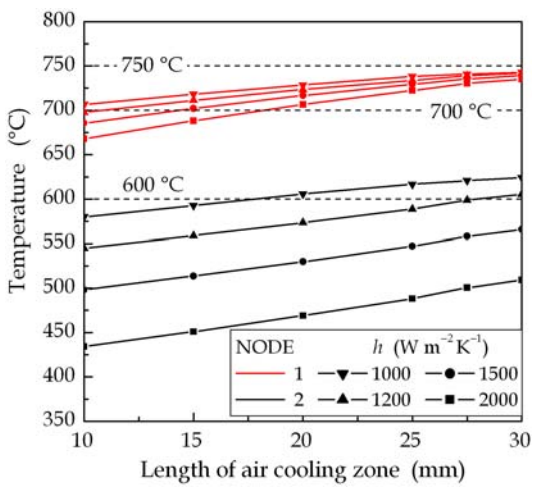

Fig. 12. Dependence of temperatures in the nodes 1 (red) and 2 (black) at the end of cooling process illustrating the influence of intensity of water spray cooling.

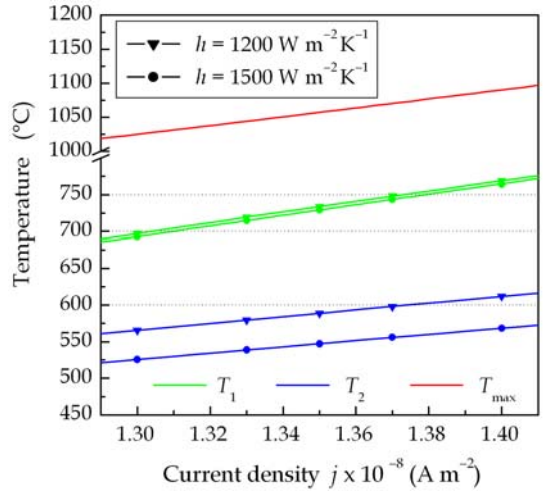

Fig. 13. Dependence of the axial temperature (node 1) and surface temperature (node 2) at the end of cooling and the maximum temperature during heating process on the current density in inductor coil.

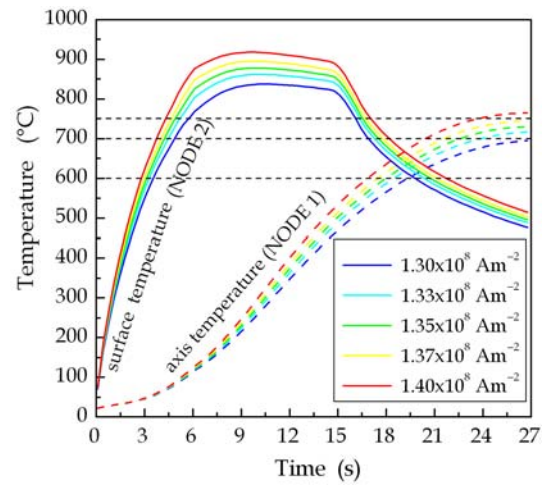

Fig. 14. Time history of the axial and surface temperatures at the billet head for chosen current densities in inductor coil.

by Jeschar et al. [25] were exploited to approximate the heat transfer coefficient in the zone of water spray cooling (Fig. 10) in dependence on the intensity of cooling given by applied water mass flow. For the supposed cooling water mass flow from 460 kg m^{-2} min^{-1} to 1000 kg m^{-2} min^{-1}, the average values of the heat transfer coefficient from 1000 W m^{-2} K^{-1} to 2000 W m^{-2} K^{-1} were used.

6. Results and discussion

Based on the presented simulation model, variant numerical experiments were performed using different parameters of induction heating and combined air and water jet cooling in order to obtain required temperature distribution before the forming process.

The length of air cooling zone b (Fig. 4) was changed from 10 mm to 30 mm. The current density in induction coil was set to the value of $j = 1.35 \times 10^8$ A m^{-2}. The water mass flow of 570 kg m^{-2} min^{-1} with corresponding average heat transfer coefficient of 1200 W m^{-2} K^{-1} was supposed in the zone of water jet cooling. The shorter air cooling zones are not advantageous as the water cooling would start before attainment of maximum temperature in the node 2 at the billet surface (Fig. 11). Elongation of the air cooling zone results in the temperature increase in the

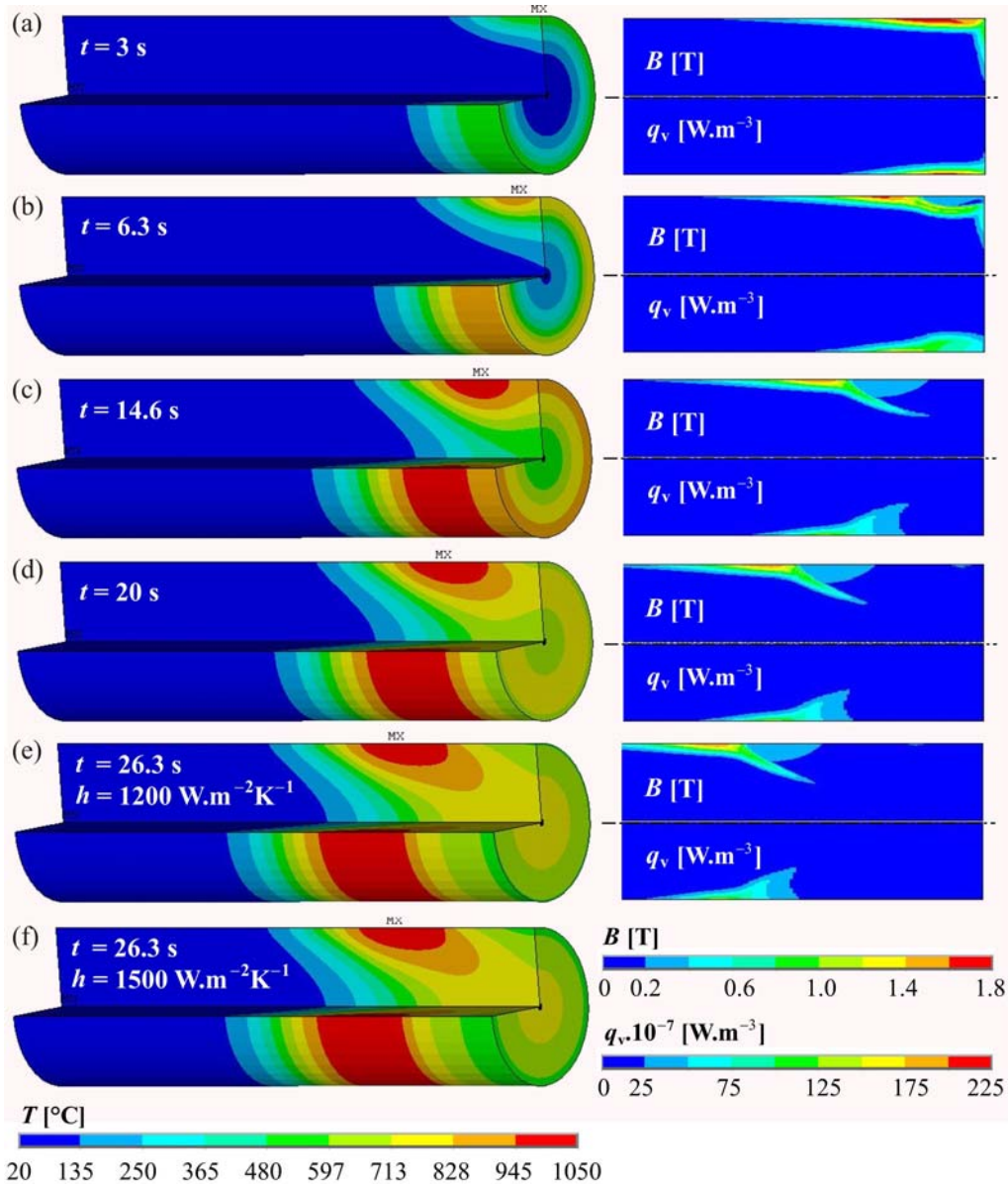

Fig. 15. Details of the temperature distribution in a billet illustrating the time sequence of heating and cooling (left) and corresponding magnetic flux density and Joule heat generation (right): (a) $t = 3$ s before temperatures exceed Curie point, (b) $t = 6.3$ s before air cooling, (c) $t = 14.6$ s at the end of air cooling, (d) $t = 20$ s during water cooling, (e) $t = 26.3$ s at the end of water cooling with $h = 1200$ W m^{-2} K^{-1}, (f) $t = 26.3$ s at the end of water cooling with $h = 1500$ W m^{-2} K^{-1}.

billet axis due to the heat conduction from billet surface parts heated by induction heating faster to its central parts. Temperatures in the node 1 at the end of cooling in the time of 26.33 s attain the values from 700 ℃ to 750 ℃ except the case with air cooling zone length of 10 mm when the axial temperature is lower than required. However, the length of water cooling zone reduced by extension of air cooling zone may not be sufficient to assure the quenching of a billet surface in the node 2 under 600 ℃.

Applying more intensive water cooling, the surface temperature at the billet head (node 2) drops but the axis temperature slightly decreases as well (Fig. 12). The influence of intensity of water jet cooling on the axis temperature at the end of cooling is not relevant for the air cooling zones with the length more than 25 mm. In this reason, the air cooling zone b with the length from 25 mm to 27 mm and corresponding water jet cooling zone c from 35 mm to 33 mm can be considered as optimal. For these lengths of cooling zones, the water mass flow from 570 kg m^{-2}min^{-1} ($h = 1200$ W m^{-2} K^{-1}) to 730 kg m^{-2} min^{-1} ($h = 1500$ W m^{-2} K^{-1}) can be recommended according to the surface temperatures at the end of cooling. The lower water mass flows are not sufficient for required surface quenching. On the

other hand, surface temperatures are too low when more intensive water cooling is applied.

The influence of current density in induction coil on the axis and surface temperatures in the nodes 1 and 2 (Fig. 13) was analysed for the zone of air cooling with the length of 25 mm and the water cooling length of 35 mm with the water jet mass flow of 570 kg m^{-2} min^{-1} and 730 kg m^{-2} min^{-1}, respectively. The increase in intensity of water cooling affects particularly billet surface temperatures. The needed current density to reach the axis temperatures from 700 ℃ to 750 ℃ attains values from approximately 1.31×10^8 A m^{-2} to 1.37×10^8 A m^{-2}. For these current densities in induction coil and considered cooling conditions, the surface temperatures in the node 2 are as required below 600 ℃. Moreover, the maximum temperatures during the heating process are lower than allowed temperature of 1200 ℃. Maximum billet temperatures are reached before starting the water cooling in the time of 14.6 s so that they are independent of the intensity of water cooling.

For needed current densities, maximum temperatures at the billet head in the node 2 from 850 ℃ to 895 ℃ were computed in the time approximately 10 s (Fig. 14) representing the surface overheating above the desired minimal axis temperature of 150 ℃ to 195 ℃.

Progress of heating and cooling processes of a rod semiproduct with time is illustrated in Fig. 15 for the current density in induction coil of 1.34×10^8 A m^{-2}. In the time of 3 s, the billet temperatures are lower than Curie point $T_C = 735$ ℃, therefore the skin depth is small. The magnetic flux density and Joule heat are concentrated in the surface layers and they achieve the maximum values during entire heating process. When the billet temperatures exceed the Curie point (Fig. 15b–f), the material becomes non-magnetic and its relative permeability falls to unity. Due to this decrease of relative permeability and increase in electrical resistivity with temperature (Table 2), the skin depth in the domains with temperatures higher than 735 ℃ enhances. The maximum temperatures under inductor at the level of 1050 ℃ are reached at the end of the air cooling process in the time of 14.6 s. After starting the water jet cooling, the billet surface temperatures decrease but the temperatures in the central parts remain to go up due to the heat conduction from the surface and middle billet parts. In the time of 20 s, the axis temperatures are lower than required. Nevertheless, the central temperatures at the end of cooling process are as desired higher than 700 ℃ for both considered intensities of water cooling (Fig. 15e,f). If higher values of the heat transfer coefficient are applied, the depth of undersurface layer chilled bellow the temperature of 600 ℃ increases from 0.75 mm for $h = 1200$ W m^{-2} K^{-1} to 5 mm for $h = 1500$ W m^{-2} K^{-1} (Fig. 16).

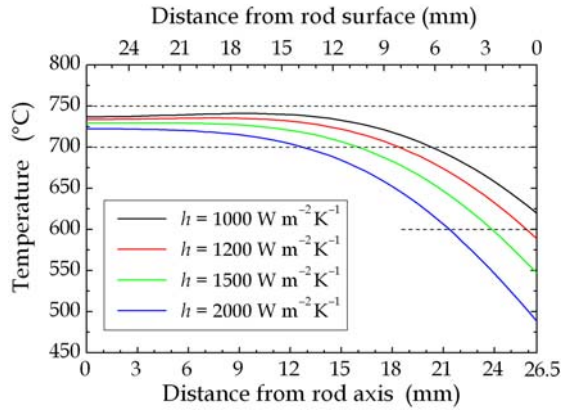

Fig. 16. Temperature distribution along the rod radius at the billet head in the time of 26.33 s (air cooling zone b = 25 mm).

7. Conclusions

The process of induction heating and combined air and water jet cooling of a rod semiproduct for the technology of rotary spin extrusion was analysed using developed simulation model and the finite element code ANSYS 10.0. Numerical experiments carried out with alternative conditions of heating and cooling proved that the required temperature distribution in the rod can be attained when appropriate inductor power, lengths of air and water cooling zones as well as sufficient intensity of water cooling are applied.

Based on the obtained results, the following parameters can be suggested for induction heating and cooling of a rod semiproduct for the feed rate of 3 mm s^{-1}:

– three-turn water cooled copper inductor coil with the frequency of 2 kHz and current density from 1.31×10^8 A m^{-2} to 1.37×10^8 A m^{-2},

– the length of air cooling by free convection and radiation b from 25 mm to 27 mm,

– the length of water jet cooling c from 35 mm to 33 mm using the mass flow from 570 kg m^{-2} min^{-1} to 730 kg m^{-2} min^{-1} providing the average heat transfer coefficient from 1200 W m^{-2} K^{-1} to 1500 W m^{-2} K^{-1}.

Acknowledgements

The authors gratefully acknowledge funding of this research work by the German Research Foundation (SFB 283), VEGA MŠ SR and SAV (1/2073/05, 1/0837/08), and the Research Centre FORTECH.

References

[1] GLASS, R.—HAHN, F.—KOLBE, M.—MEYER, L. W.: Journal of Materials Processing Technology, *80–81*, 1998, p. 174.

[2] NEUGEBAUER, R.—KOLBE, M.—GLASS, R.: Journal of Materials Processing Technology, *119*, 2001, p. 277.

[3] NEUGEBAUER, R.—KOLBE, M.—GLASS, R.: Production Engineering, Research and Development, *8*, Book 2, 2001, p. 29.

[4] NEUGEBAUER, R.—MAHN, U.—WEIDLICH, D.: Konstruktion, *9*, 2001, p. 55.

[5] NEUGEBAUER, R.—GLASS, R.—KOLBE, M.—HOFFMANN, M.: Journal of Materials Processing Technology, 2002, p. 856.

[6] http://www.iwu.fraunhofer.de [online], [cit. 2006-04-15; 10:08 SEČ]

[7] MICHEL, R.—KREIßIG, R.—ANSORGE, H.: Forschung im Ingenieurwesen, *68*, 2003, p. 19.

[8] MAŠEK, B.—MEYER, L. W.—NOVÝ, Z.: In: International Conference PEDD 6, Egypt, Cairo Ain Shams University 2002.

[9] MEYER, L. W.—MAŠEK, B.: In: 8th Saxon Conference of Forming Technology, Freiberg, TU-BA 2001, p. 176.

[10] JANDOVÁ, D.—MEYER, L. W.—MAŠEK, B.—NOVÝ, Z.—KEŠNER, D.—MOTYČKA, I.: Materials Science and Engineering, *A349*, 2003, p. 36.

[11] JANDOVÁ, D.—ŘEHOŘ, J.—NOVÝ, Z.: Journal of Materials Processing Technology, *157–158*, 2004, p. 523.

[12] MAŠEK, B.—NEUGEBAUER, R.—MAHN, U.—MEYER, L. W.: Stahl und Eisen, *124*, 2004, p. 77.

[13] STAŇKOVÁ, H.—MAŠEK, B.—MEYER, L. W.: In: 7th International Conference on Production Engineering and Design for Development, Cairo, PEDD 2006.

[14] HAIMBAUGH, R. E.: Practical Induction Heat Treating. ASM International 2001.

[15] LANGER, E.: Teorie indukčního a dielektrického tepla. Praha, Academia 1979.

[16] NOVÁK, P.: Základy elektrotepelnej techniky. Košice, Mercury-Smekal 2001.

[17] INCROPERA, F. P.—DE WITT, D. P.: Fundamentals of heat and mass transfer. New York, J. Wiley and Sons 1996.

[18] TARABA, B.—BEHÚLOVÁ, M.—KRAVÁRIKOVÁ, H.: Mechanika tekutín a termomechanika. Bratislava, ES STU 1999.

[19] Ansys Theoretical Manual, Release 10.0, SAS IP, Inc., 2005.

[20] BEHÚLOVÁ, M.—MAŠEK, B.—MEYER, L. W.: MP-Materialprüfung, *48*, 2006, p. 217.

[21] BEHÚLOVÁ, M.—MAŠEK, B.—MEYER, L. W.: Virtual testing of the dynamic induction heating. Finite Elements in Analysis and Design (to be published).

[22] TARABA, B.: Numerical analysis of temperature fields and its application in chosen technological processes. [Assoc. Prof. Graduation Work]. Košice, TU 2003.

[23] ELFMARK, J. et al.: Metal Forming. Prague, SNTL 1992.

[24] BEHÚLOVÁ, M.: Research Papers. Trnava, MtF STU, Vol. 15, 2003, p. 9.

[25] JESCHAR, R.—SPECHT, V.—HEIDT, V.: In: Braunschweigischen Wissenschaftlichen Geselschaft, Göttingen, Verlag Erich Goltze 1991. PMid:20305743